Mass transfer enhancement for CO2 chemical absorption in a spiral baffle embedded microchannel

Hao Cheng, Dominique Tarlet, Yilin Fan, Lingai Luo

Mass transfer enhancement for CO_2 chemical absorption in a spiral baffle embedded microchannel

Hao CHENG[a], Dominique TARLET[a], Yilin FAN[a,*], Lingai LUO[a,†]

[a] *Nantes Université, CNRS, Laboratoire de Thermique et Energie de Nantes, LTeN, UMR 6607, F-44000 Nantes, France*

Abstract: This paper presents an experimental study on CO_2 chemical absorption by Monoethanolamine (MEA) solution in microchannel. In particular, a novel spirally distributed baffle structure is proposed to be embedded into the microchannel so as to generate the swirling flow pattern and to enhance the mass transfer. The effect of spiral baffle structure on the two phase flow pattern transition, the CO_2 gas void fraction, the pressure drop, and the mass transfer performance are characterized and discussed, under varied gas and liquid flow rates, and MEA concentrations. Results demonstrate that the spiral baffle structure could significantly enhance the gas-liquid mass transfer, with overall liquid side volumetric mass transfer rate (k_La) up to 2.35 s^{-1} and enhancement number E up to 1.387 at small gas and liquid Reynolds numbers (Re_G<5.5; Re_L<14). New predictive correlations have also been proposed by considering both the structure enhancement factor and the chemical reaction factor.

Keywords: Microchannel, spiral baffle, gas-liquid two-phase flow, mass transfer enhancement, carbon capture, CO_2 chemical absorption

* Corresponding author. E-mail address: Yilin.fan@univ-nantes.fr (Y. Fan)

† Corresponding author. E-mail address: lingai.luo@univ-nantes.fr (L. Luo)

Nomenclature

A	Mass transfer interface area (m^2)
a	Specific interface area (m^{-1})
C_{MEA}	MEA volumetric concentration
C^*	CO_2 equilibrium concentration ($mol.m^{-3}$)
D	Diffusion coefficient (m^2s^{-1})
d_h	Hydraulic diameter (m)
E	Enhancement number
Ec	Energy consumption ratio
f	Frequency
H	Henry constant ($mol.m^{-3}.Pa^{-1}$)
k_{ov}	Overall reaction rate (s^{-1})
k_L	Liquid side mass transfer coefficient ($m.s^{-1}$)
$k_{L,P}$	Liquid side physical mass transfer coefficient ($m.s^{-1}$)
l	Length (m)
n	Molar mass (mol)
r	fillet radius
R	Gas constant ($J.mol^{-1}K^{-1}$)
P	Pressure (Pa)
Q	Volumetric flow rate ($ml.h^{-1}$)
T	Experimental temperature (K)
t	Absorption duration time (s)
U	Superficial velocity ($m.s^{-1}$)
V	Volume (m^3)
w	Microchannel width (m)

Greek symbols

δ_0	Liquid film thickness (m)
μ	Dynamic viscosity (Pa.s)
σ	Surface tension ($N.m^{-1}$)
$\boldsymbol{\rho}$	Density ($kg.m^{-3}$)
β	Dimensionless ratio of gas-liquid flow rate
$\boldsymbol{\Delta}$	Difference
Ψ	Intensified structure number
ε	Gas void fraction
$\emptyset$	Relative uncertainties
η	Effective energy efficiency

Dimensionless number

Ca	Capillary number, $Ca = \mu U/\sigma$
Da	Damköhler number, $Da = k_{ov} \cdot {d_h}^2/D$
Ha	Hatta number, $Ha = \sqrt{D\,{k_{ov}/k_{L,p}}^2}$
Re	Reynolds number, $Re = \rho U d_h/\mu$
Sh	Sherwood number, $Sh = k_L d_h/\mathrm{D}_{AB}$
Sc	Schmidt number, $SC = \mu_L/\mathrm{D}_{AB} \cdot \rho_L$
We	Weber number, $We = \rho U^2 d_h/\sigma$

Subscripts

B	Bubble
C	Channel
G	Gas
L	Liquid
in	Inlet
ini	Initial
out	Outlet

1. Introduction

The increase of CO_2 concentration in atmosphere is one of the main causes of global warming, whose disastrous consequences have been well recognized (Florides and Christodoulides, 2009) (Shakun et al., 2012). The development and implementation of efficient CO_2 capture technologies receive much more attention nowadays, aiming at the Carbon neutrality target by year 2050 (Schreyer et al., 2020). Conventional CO_2 capture methods include chemical absorption, physical absorption or adsorption, membrane separation, cryogenic distillation, etc. (Koytsoumpa et al., 2018; Lamb, 2017; Murai and Fujioka, 2008; Stewart and Hessami, 2005). Among them, the chemical CO_2 absorption method has shown to be an adapted and widely used one for large-scale industrial application, such as for power plant flue CO_2 treatment. But this method usually involves voluminous equipment, inevitably bringing some problems such as high investment costs, huge amount of absorbent needed, high energy consumption, and relatively low mass transfer performance. These drawbacks may be solved through the miniaturization, more precisely by the employment and implementation of micro-structured absorbers/reactors (Lin et al., 2019; Mc Carogher et al., 2021). The channel characteristic size of the microreactor is usually in the order of tens to hundreds of microns, greatly increasing the specific interfacial area for mass transfer. Owing to this benefit, numerous studies have been conducted on the microchannel based CO_2 chemical absorption over the past decades (Zanfir et al., 2005; TeGrotenhuis et al., 2000), the latest advances are summarized in recent review papers (Cheng et al., 2023; Pasha et al., 2022). However, some limitations still exist, mainly due to the laminar regime of two-phase flow at small Reynolds numbers (*Re*) of liquid and gas in the microchannel. The diffusion dominates the mass transfer between CO_2 bubble and the liquid solvent, restraining the absorption performance. In brief, researches are still needed on the microchannel-based CO_2 absorbers for performance improvement (Ma et al., 2020; Tan et al., 2012).

In this context, many intensification measures have been proposed, implemented and tested, working either on the global geometry (Pang et al., 2021) or inner structure of the microchannel (Chen et al., 2019), or on some special operational modes (Dong et al., 2015). Among these methods, installing flow disturbance structures in the microchannel could induce the local eddy

flow and deform the gas-liquid interface, thereby constituting an effective and economic way to improve the CO_2 absorption performance. A number of experimental studies have been performed with different channel and obstacle geometries (micro grooves, micro protrusions, etc.), as summarized in Table 1. For example, Zhang et al. (2021) proposed the sudden expansion microstructure accompanied microchannel to enhance the gas-liquid interface disturbance. Their results showed that the liquid side volume mass transfer rate ($k_L a$) could be increased by a factor of 2.4. In particular, rectangular-shape baffle structure has been applied for the mass transfer enhancement. Yin et al. (2020) fabricated a rectangular microchannel with staggered rectangular baffles and investigated the effect of baffle parameters (length, arrangement, etc.) on the CO_2/water mass transfer performance. Their results showed that the $k_L a$ could be augmented by a factor of 2.8 owing to the baffle structure. Recently, Yin et al. (2022a) proposed a continuous sudden expansion microchannel structure accompanied with rectangular obstacles in the middle (cf. Table 1) to create the bubble flow splitting and recombining. Their results demonstrated that the $k_L a$ could be increased by 2.74 times.

All these studies have verified the intensified CO_2 absorption performance by obstacle structures, but at the cost of an increased pressure drop. Further optimizing the obstacle structure embedded microchannel to intensify the mass transfer with a reasonable increase of pressure drop is a key issue in this field. This is especially true for small gas/liquid *Re* number operation for which the mass transfer is rather limited but interesting in terms of low presure loss. The enhancement of mass transfer by proper obstacle geometry and arrangement is of great practical significance, but systematic researches on this topic are more than needed. Besides, for CO_2 chemical absorption in microchannel, the conventional correlations based on common physical dimensionless numbers for the prediction of gas-liquid mass transfer performance become less applicable. Some new correlations considering the effect of chemical reaction have been proposed, showing better prediction accuracy. Nevertheless, the introduction of chemical reaction factor into the correlations is still complicated, letting alone the prediction of additional enhancement effect by flow disturbance structures.

In this work, we propose a novel spiral baffle structure embedded into the microchannel to

intensify the CO_2 chemical absorption at small gas and liquid *Re* numbers. The spirally distributed obstacles at the inner walls of microchannel are expected to generate a swirling flow pattern and more spatially asymmetric vortices in liquid phase to enhance the mass transfer. The comparative experimental study of CO_2 absorption in Monoethanolamine (MEA) solvent in a spiral baffle embedded microchannel and in a smooth microchannel was performed. The influence of spiral baffle structure on the two-phase flow pattern, the gas void fraction, the pressure drop, and the CO_2 absorption rate were experimentally investigated under a varied gas and liquid flow rates and MEA concentrations. Based on the obtained experimental data, new correlations were also proposed for predicting the liquid side volumetric mass transfer rate by considering both the structure enhancement factor and the chemical reaction factor, more appropriate for the cases like CO_2 chemical absorption in structured microchannels. Furthermore, the energy consumption of the CO_2 absorber with enhancement structure were evaluated. The obtained results could contribute to the potential industrial application of mini-microchannel reactors for carbon capture.

Table 1. A summary of recent microchannel based CO_2 absorption enhancement studies by embedded obstacle structures

Study	Two-phase flow system	Operating range	Flow pattern/working conditions	Microchannel geometry & dimension (mm)	Intensification measure	Structure diagram	k_La improvement
Chen et al. (2021)	CO_2 [Bmim][BF_4] aqueous	Q_L: $50-80$ ml/h Q_G: $80-360$ ml/h	Slug flow 298.15 ± 1 K Ambient pressure	T-type rectangular straight microchannel 0.4×0.8×35.2	0.1 mm thickness heart-shaped groove	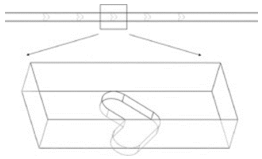	2.2 times
Yin et al. (2020)	CO_2 Water	U_L: $0.043-0.07$ m/s U_G: $0.017-0.26$ m/s	Slug/broken slug flow 298.15 K Ambient pressure	T-type rectangular straight microchannel 0.8×0.8×30.4 0.6×0.6×30.4 0.4×0.4×30.4	Staggered rectangular baffles	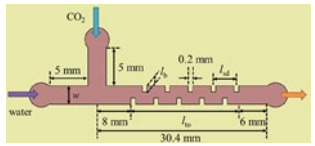	2.8 times
Yin et al. (2022a)	CO_2 AMP aqueous	Q_L: $40-100$ ml/h Q_G: $20-500$ ml/h	Complete/partial breakup 293.15 K Ambient pressure	Optimized T-type rectangular straight microchannel 0.4×0.6×25	Split–and–recombine structure	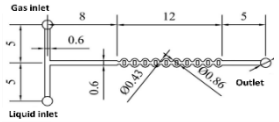	2.74 times
Zhang et al. (2021)	CO_2 [Bmim][BF_4] aqueous	Re_L: $1.67-27.22$ Re_G: $11.81-32.30$	Slug/slug-bubbly flow 298.15 K Ambient pressure	T-type rectangular straight microchannel 0.4×0.4×34	Sudden expansion structure	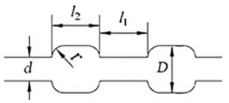	2.4 times
Yin et al. (2019b)	CO_2 [Bmim][BF_4] MEA aqueous	Q_L: $30-60$ ml/h Q_G: $20-500$ ml/h	Slug/broken slug/slug-bubbly flow 298.15 K Ambient pressure	T-type rectangular straight microchannel 0.4×0.8×30.4	Up-down embedded baffles	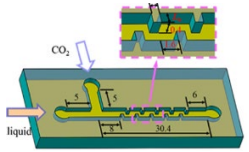	1.5 times
Nie et al. (2022)	CO_2 [Bmim][BF_4] aqueous	Q_L: $50-80$ ml/h Q_G: $40-220$ ml/h	Slug/broken slug flow 298.15 K Ambient pressure	T-type rectangular straight microchannel 0.8×0.8×30.4	Up-down embedded triangular obstacles	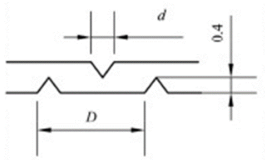	2.1 times

2. Methodology

2.1 Experimental setup and microchannel reactor

Fig. 1a shows the experimental setup used for this study. CO_2 (Air Liquide, France, 99.9% purity) was used as the gas phase and its flow rate was controlled by a mass flow controller (Brooks SLA 5850). MEA (Arcane-industries, France, 99.9% purity) solution was used as the liquid phase and was delivered at constant flow rate by a micro syringe pump (kdScientific-267, 1% uncertainty). A camera with 4112×3008 -pixel resolution (Basler acA4112-30μm) equipped with lens (EDMUND optical 50mm/F2.0 59873, USA) was used to monitor and record the two-phase flow in microchannel after the two-phase flow pattern and pressure reached steady. The camera was operated at a frame rate of 30 fps. Basler video recording software was used to control and adjust the image parameters captured by high resolution camera. A 36w flat uniform cold light source (LED panel from LEDVANCE) was positioned close behind the microchannel to provide background illumination during images recording process. A pressure gauge (Kobold Pad FEE 3S2NS00 series) was installed at the gas inlet port to measure the pressure drop, while the pressure at the outlet was estimated as atmospheric pressure. The measuring range and precision of these instruments are given in Table 3.

Two microchannel reactors (absorbers) were tested and compared in this study for CO_2 chemical absorption: one smooth straight microchannel and another with intensification structure. Both microchannels have a square cross-section of 1 mm × 1 mm, the length of main channel being 90.5 mm. A T-type junction was designed for gas-liquid contact. The inlet branches have the same cross-section dimension as the main channel, and the length for each inlet branch is 10 mm. For the microchannel with intensification structure, three spiral baffle groups were embedded in the main channel. Each baffle group consists of 4 small cubes (0.5 mm side), arranged in rotation and quarterly distributed in the inner walls of the microchannel with 3 mm spacing (Fig. 1b). Such novel baffle structure is intended to create the swirling flow and the spatial asymmetric two-phase interface disturbance, so as to enhance the mass transfer. A space of 15 mm was left between the second and the third group, for better recognizing the bubble volume changes after passing through the first two groups which were successively

arranged. More details about the geometry and dimensions of the microchannel with intensification structure can be found in Fig. 1b.

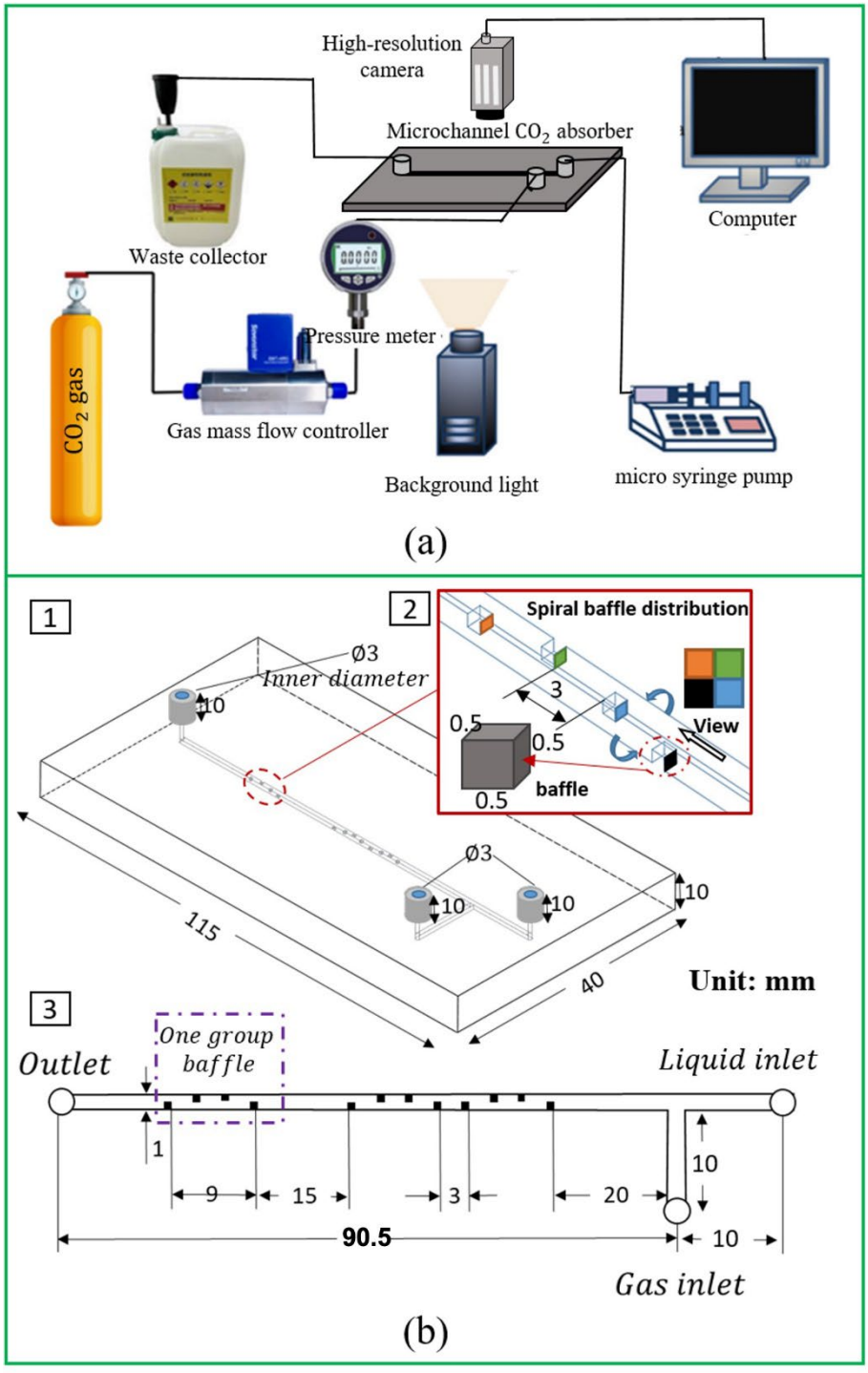

Figure 1 Schematic diagram of the experimental setup. (a) the test-rig; (b) 3-D diagram of spiral baffle embedded microchannel.

Both microchannel absorber prototypes (Fig. 1b) were realized with transparent resin

(WaterClear) using laser stereolithography. In this process, photopolymer was cured selectively at the local focus of ultraviolet laser. The external walls of the prototypes were further polished for better transparency.

The tested flow rate range was 12-168 *ml/h* for the gas phase and 10 – 50 *ml/h* for the liquid phase, respectively. The corresponding *Re* number ($Re = \rho U d_h/\mu$) range was 0.42-5.51 (for gas) and 2.78-13.9 (for liquid), respectively. Note that ρ is the density (kg/m^3), U is the superficial velocity (m/s), d_h is the hydraulic diameter of the main microchannel (m) and μ is the dynamic viscosity $(Pa \cdot s)$. Experiments were performed using MEA solution with three different concentrations, i.e., $C_{MEA} = 1\%;\ 3\%$ and 5% vol.

All experiments were conducted under ambient temperature (293 K) and pressure. For each measurement, it took about 10 min for the stabilization of two-phase flow. The gas-liquid two-phase flow patterns observed and the absorption performance show good stability and reproducibility, which will be presented in section 3.1.

2.2 Chemical reaction theory

The CO_2 chemical absorption by MEA can be characterized by zwitterion mechanism (Lv et al., 2015). Several principal reaction steps could occur in the CO_2-MEA-H_2O absorption system. Firstly, the MEA molecules quickly react with CO_2 to form intermediate zwitterion (Eq. 1). Then the zwitterion is quickly neutralized to form carbamate (Eq. 2). The whole process can be combined as carbamate formation and expressed as Eq. 3.

$$CO_2 + R'NH_2 = R'NH_2{}^+COO^- \quad (1)$$

$$R'NH_2{}^+COO^- + R'NH_2 = R'NHCOO^- + R'NH_3{}^+ \quad (2)$$

$$CO_2 + 2R'NH_2 = R'NHCOO^- + R'NH_3{}^+ \quad (3)$$

Where R' is CH_2CH_2OH, $R'NH_2{}^+COO^-$ and $R'NHCOO^-$ are the zwitterion and the carbamate, respectively. Meanwhile, $HCO_3{}^-$ is formed by the CO_2 hydration under high CO_2 loading (Eq. 4) and accompanied by the hydrolysis of carbamate (Eq. 5).

$$CO_2 + H_2O + R'NH_2 = HCO_3^- + R'NH_3^+ \quad (4)$$

$$CO_3^{2-} + H^+ + R'NH_2 = \quad R'NHCOO^- + H_2O \quad (5)$$

For CO_2 desorption, the carbamate is decomposed into MEA and CO_2 under heating condition and the solvent is regenerated (Eq. 6).

$$R'NHCOO^- + H^+ \xrightarrow{heating} R'NH_2 + CO_2(g) \quad (6)$$

The chemical reaction rate of MEA-CO_2 is fast enough, so that the CO_2 concentration in bulk MEA solution is considered to be '0'.

Different MEA concentrations have been used in this study. The physicochemical properties are listed in Table 2. Note that the diffusion coefficient (D) and overall chemical reaction rate (k_{ov}) of CO_2- MEA solution reaction system are refer to papers (Yin et al., 2019a).

Table 2. Physicochemical properties of CO_2- MEA solution reaction system

C_{MEA}	Density $\rho_L(\mathrm{kg/m^3})$	Viscosity $\mu_L \times 10^3(\mathrm{Pa.s})$	Diffusivity $D \times 10^9(\mathrm{m^2/s})$	Chemical reaction rate $k_{ov}(\mathrm{s^{-1}})$
1%	998.6	0.978	1.99	451.06
3%	998.9	0.986	2.03	1403.18
5%	999.1	1.041	2.08	2355.24

2.3 Calculation of bubble volume and surface area

The variation of CO_2 bubble volume and surface area over time in microchannel are key parameters for the evaluation of absorption performance. In this study, the optical capturing and image processing method has been used to acquire the transient bubble geometry and dimensions. For slug flow, a single CO_2 bubble was treated as 'two hemisphere caps + symmetrical main body', as shown in Fig. 2(a). The thickness of liquid film between the bubble and the channel wall can be estimated as (Youn et al., 2015):

$$\frac{\delta_0}{d_h} = \frac{0.67Ca^{2/3}}{3.13Ca^{2/3}+1+0.504Ca^{0.672}Re_L{}^{0.589}-0.352We^{0.629}} \quad (Ca < 0.04,\ Re_L < 2000) \tag{7}$$

Where Ca is the capillary number ($\mu U/\sigma$) and We is the Weber number ($\rho U^2 d_h/\sigma$), respectively. σ is the two-phase surface tension (N/m).

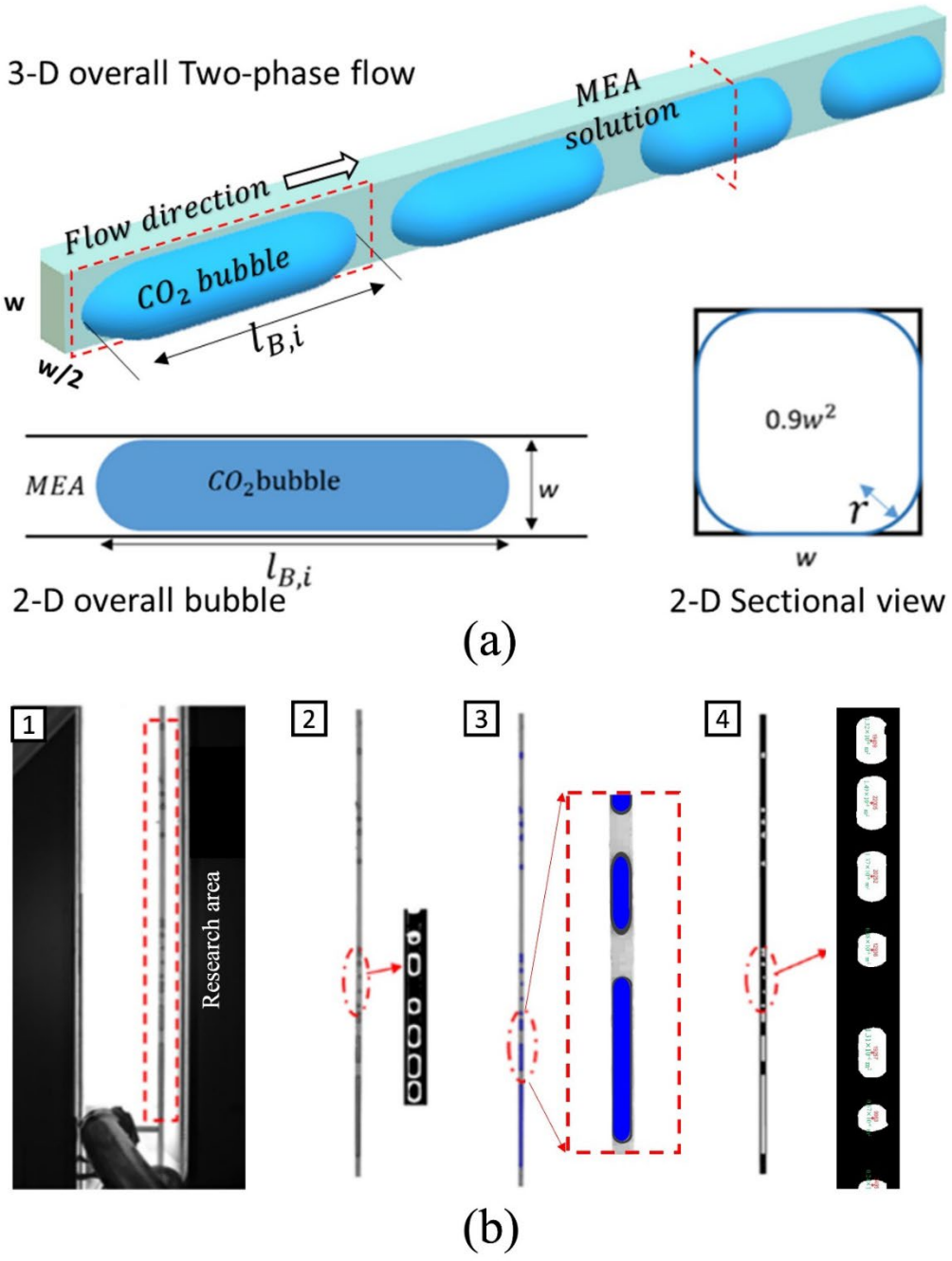

Figure 2 Image processing for the calculation of bubble volume and surface area. (a) Schematic diagram of gas-liquid two-phase flow in microchannel. (b) MATLAB based image processing method

For this study ($Ca < 1 \times 10^{-3}$, Re_L<15), the dimensionless liquid film thickness (δ_0/d_h) is estimated to be smaller than 6.5×10^{-3}, thus could be neglected in the calculation of bubble volume and interfacial area. The bubble cross sectional area is estimated to be equal to $0.9w^2$ (Zhu et al., 2017). The single slug bubble volume ($V_{B,i}$) and surface area ($A_{B,i}$) are then decided by the bubble length, calculated as follows:

$$V_{B,i} = \frac{\pi w^3}{6} + 0.9w^2\left(l_{B,i} - w\right) \quad l_{B,i} > w \tag{8}$$

$$V_{B,i} = \frac{\pi {l_{B,i}}^3}{6} \quad l_{B,i} \le w \tag{9}$$

$$A_{B,i} = \pi w^2 + (2\pi r + 4w - 8r)\left(l_{B,i} - w\right) \quad l_{B,i} > w \tag{10}$$

$$A_{B,i} = \pi {l_{B,i}}^2 \quad l_{B,i} \le w \tag{11}$$

The bubble length ($l_{B,i}$) and the fillet radius (r) were obtained by analyzing the two-phase flow pictures captured by high-resolution camera using MATLAB (v2020a) tools, as explained in Fig. 2b. The original RGB images were converted to gray images and the two-phase flow areas were extracted by MATLAB. The gas-liquid interface was identified by using edge recognition algorithm 'Sobel'. Then the interface gray image was converted to black-white binary image to reduce the image background noise. In order to verify the processed result, the recognized bubble area was compared with the original images. Since the size and the scale of the pixels are known, the 2-D bubble size parameters could be acquired by counting the number of pixels in every single bubble. The real bubble instantaneous volume and surface area could then be calculated based on Eqs. 8-11.

2.3 Mass transfer calculation

For single CO_2 bubble, the reduction of CO_2 molecules ($\Delta n_{co_2}, mol$) can be expressed by:

$$\Delta n_{co_2} = \frac{P_{in}V_{in} - P_{out}V_{out}}{RT} \tag{12}$$

Where R $(J/mol \cdot K)$ is the ideal gas constant, T (K) is the working temperature, P_{in} (Pa)

is the gas pressure at microchannel inlet measured by pressure gauge, P_{out} (Pa) is the pressure at microchannel outlet (estimated as atmosphere pressure), V_{in} (m^3) is the initial bubble volume and V_{out} (m^3) is the bubble volume at the end of microchannel.

Two-film model (Kashid et al., 2011) is used for mass transfer calculation, assuming that there are a gas stagnant layer (gas film) and a liquid stagnant layer (liquid film) on each side of the gas-liquid interface. For quick chemical reaction and pure CO_2 gas phase, the liquid-side mass transfer resistance is dominant while the gas-side mass transfer resistance can be ignored (Whitman, 1923). Therefore, the Δn_{CO_2} for a single CO_2 bubble could also be calculated as:

$$\Delta n_{CO_2} = A_{B,i} k_{L,i} (C^* - C_{CO_2}) t \tag{13}$$

Where k_L (m/s) is the liquid side mass transfer coefficient, t (s) is the absorption duration, C^* (mol/m^3) is the equilibrium CO_2 concentration in MEA solution which is decided by Henry's law. C_{CO_2} is the CO_2 concentration in liquid slug at *t* time (estimate as 0). Thus, for a single bubble, the volumetric mass transfer rate $k_{L,i}a_i$ (s^{-1}) could be calculated as follows:

$$k_{L,i}a_i = \frac{P_{in}V_{in} - P_{out}V_{out}}{V_C C^* t R T} \tag{14}$$

$$C^* = P_{CO_2} \times H \tag{15}$$

Where a_i $(1/m)$ is the specific surface area of single bubble which is defined as $A_{B,i}/V_C$, V_C is the microchannel volume, P_{CO_2} is the average CO_2 pressure in microchannel, calculated as:

$$P_{CO_2} = \frac{\ln(\frac{P_{in}}{P_{out}})}{P_{in} - P_{out}} \tag{16}$$

H is *Henry's* constant estimated to be 3.78×10^{-4} $(mol/m^3.Pa)$ (Versteeg and Van Swaaij, 1988).

For continuous and stable slug flow in microchannel, the initial CO_2 bubble volume (V_{in}) and bubble generation frequency (f_{CO_2}) could be estimated as constant. Thus, the overall liquid

side volumetric mass transfer rate k_La (s^{-1}) could be calculated as:

$$k_La = \frac{(P_{in}V_{in} - P_{out}V_{out}) \cdot f_{CO_2}}{V_C C^* tRT} \quad (17)$$

2.5 Uncertainty Analysis

The estimated uncertainties of experimentally measured parameters and calculated results are listed in Table 3. The CO_2 mass flow controller (Brooks SLA 5850) and the syringe pump (kdScientific-267) were calibrated by standard volumetric method and the relative uncertainties are $\pm$0.03 ml/min and $\pm$0.1 ml/h, respectively. The experimental temperature was measured by a calibrated K-type thermocouple with uncertainty of $\pm$0.5 K. The uncertainties of calculated parameters were estimated based on error propagation method (Moffat, 1988). In this study, the bubble parameters were captured by high-resolution camera and used to calculate the $V_{B,i}$. The largest uncertainty is 2 pixels (66 μm) and its contribution to the relative uncertainties ($\emptyset$) of $V_{B,i}$ is showed in Fig. 3. With the decrease of bubble volume, the relative uncertainty becomes much larger. The initial bubble length is larger than 5 mm under the tested conditions and the maximum relative uncertainty of bubble volume is estimated to be smaller than ±4% (Fig. 3a). The uncertainty of CO_2 gas phase void fraction (ε) could be caused by microchannel fabrication inaccuracy and $V_{B,i}$. The dimension error due to 3D printing is estimated to be in the order of 0.05 mm which can be ignored regarding the whole microchannel volume. The relative uncertainty of ε is thereby estimated to be equal to that of bubble volume. Under the testing range of this study, the bubble volume change is smaller than 4.9×10^{-9} m^3 and the relative uncertainty of k_La (Eq. (17)) is estimated to be $\pm$ 3%. With the increase of Q_G, the uncertainty of k_La could gradually decrease and become smaller than ±1% (Fig. 3b). The uncertainty for the enhancement number E $((k_La)_{structured}/(k_La)_{smooth})$ is decided by $\emptyset$ (k_La) and its maximum value is estimated to be $\pm$ 6.21%.

Table 3 Estimated uncertainties of measured and calculated parameters

Measured parameter		Uncertainty
Liquid volumetric flow rate	Q_L	±0.1 ml/h
Gas volumetric flow rate	Q_G	±0.03 ml/min
Pressure drop	ΔP	±5.6 Pa
High speed camera pixels	-	2 pixels (±66 μm)
Experimental temperature	T	±0.5 K
Calculated parameters		**Uncertainty**
Initial single bubble volume	$V_{B,i}$	±3.91%
Void fraction	$\mathcal{E}$	±3.91%
Liquid side volumetric mass transfer rate	$k_L a$	±3.01%
Enhancement number	E	±6.21%

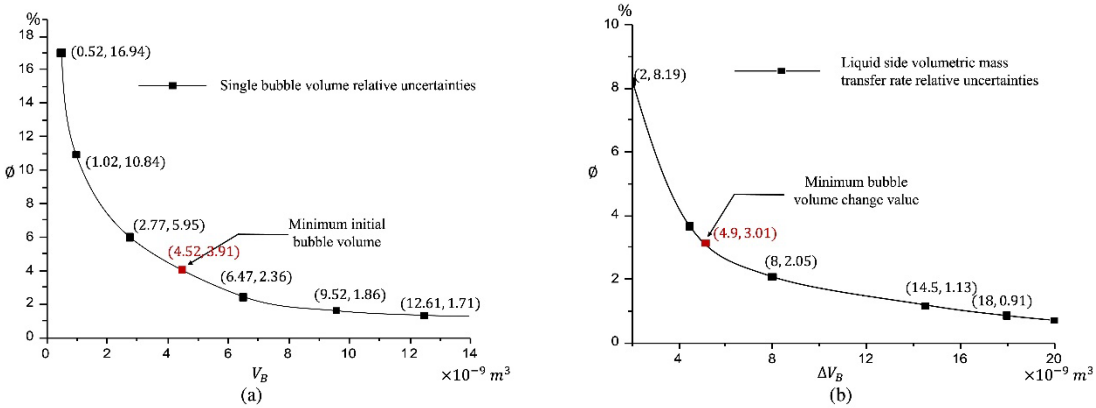

Figure 3 Range of relative uncertainties for calculated parameter. (a) Single bubble volume $V_{B,i}$; (b) Liquid side volumetric mass transfer rate $k_L a$.

3. Results and discussion

3.1 Two-phase flow pattern

The gas-liquid two-phase flow pattern plays a determinant role on the mass transfer characteristics of CO_2 chemical absorption in microchannel (Niu et al. 2009). The chemical reaction accompanied two-phase flow patterns become much more complex because of the enhanced mass transfer dynamics. In this study, CO_2 chemical absorption has been performed in two above-presented microchannels. According to the changes of bubble shape along the

microchannel, various two-phase flow patterns were captured under the tested flow rate conditions, including bubbly flow, slug-bubbly flow, slug flow, and slug-annular flow. Some typical flow patterns are shown in Fig. 4 (C_{MEA}: 5% $vol.$) and briefly described below.

Bubbly flow: This flow pattern appears at low Q_G and high Q_L with short initial bubble length ($l_{B,ini} < 5d_h$). Due to the fast chemical reaction accompanied mass transfer, the gas bubble quickly shrinks into a small bubble within a very short distance from the junction.

Slug-bubbly flow: With the increase of Q_G, the initial bubble has a longer length. the initial two-phase flow pattern shows slug flow pattern and gradually transits to bubbly flow due to the chemical absorption.

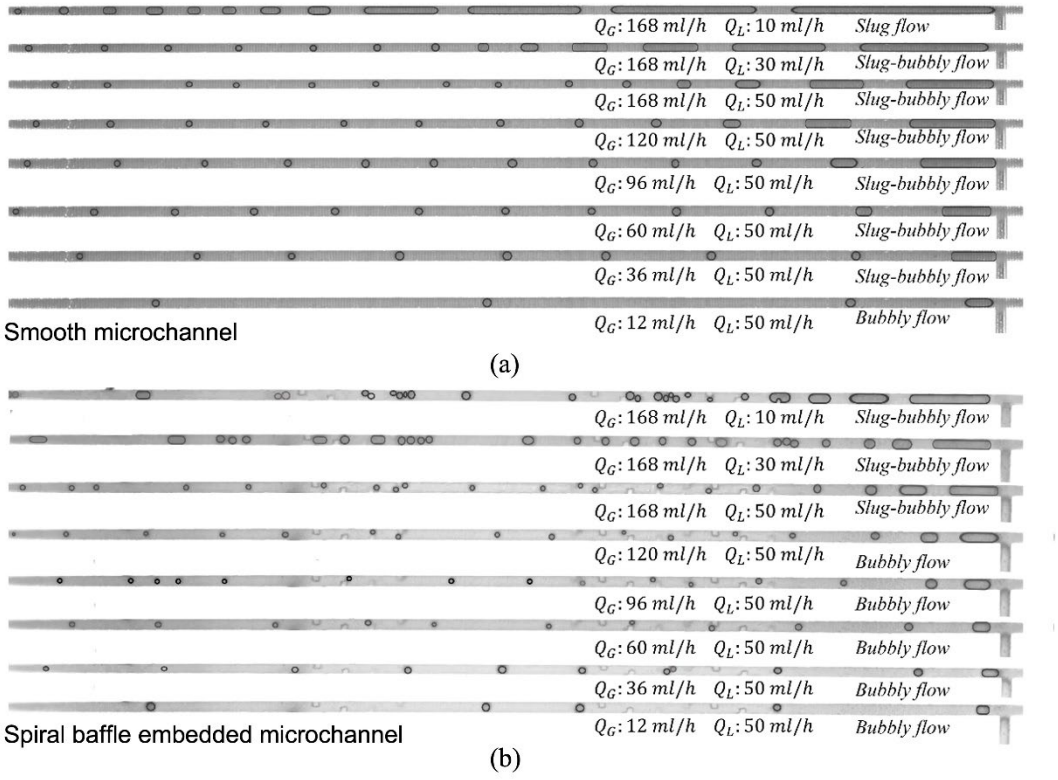

Figure 4 Typical gas-liquid two phase flow patterns for CO_2 chemical absorption (C_{MEA}: 5% vol.). (a) Smooth microchannel; (b) Spiral baffle embedded microchannel

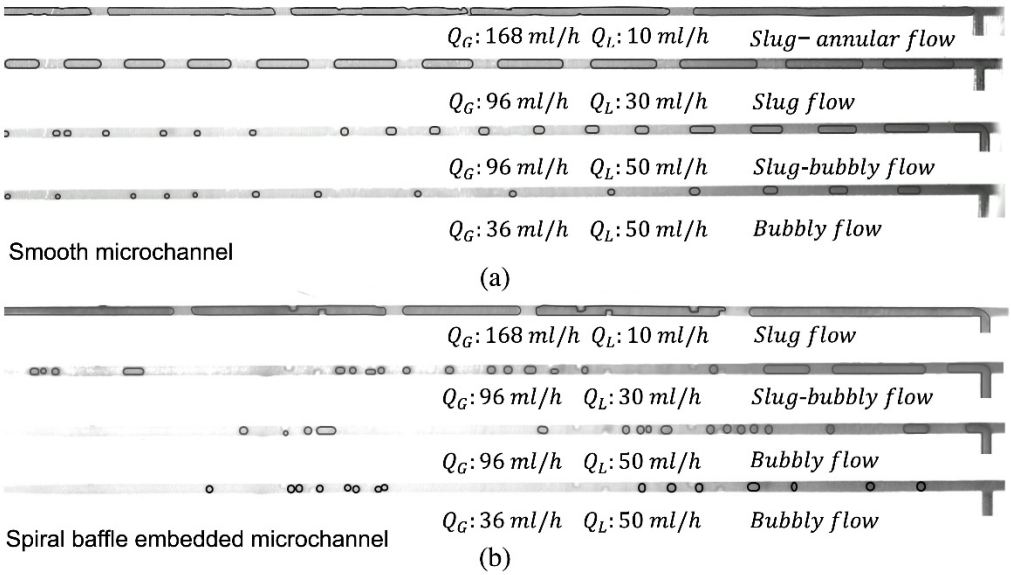

Figure 5 Typical gas-liquid two phase flow patterns for CO_2 chemical absorption (C_{MEA}: 1% vol.). (a) Smooth microchannel; (b) Spiral baffle embedded microchannel

Slug flow: This flow pattern occurs at the higher Q_G and the lower Q_L in the microchannel without baffle (e.g., $Q_G > 100\ ml/h$ and $Q_L = 10\ ml/h$). In this situation, the $l_{B,ini}$ largely increases while the liquid-side mass transfer coefficient is limited. As a result, slug flow pattern persists along the microchannel. But the situation is different in spiral baffle embedded microchannel, which will be discussed later.

Slug-annular flow: At still higher Q_G and low Q_L, the liquid slug length obviously decreases, and gas slugs could merge together. In our study, this slug-annular flow pattern has only been observed in smooth microchannel with $C_{MEA} = 1\%$ (Fig. 5) when Q_L is 10 ml/h and Q_G larger than 140 ml/h. Under the same condition, the slug flow has always been observed in the spiral baffle embedded microchannel.

Besides, the bubble deformation due to the baffle structure was observed, as shown in the images captured with 16x lens in Fig. 6. When bubble passes through the spiral baffle structure, the bubble cap is squeezed and asymmetrically deformed. The quarterly rotational distribution of baffle cubes generates the swirling pattern of the gas bubble. In the meantime, the secondary

flow of the liquid phase could also be generated, especially close to the bubble caps where the mass transfer is the most intensive. In this way, the liquid side mass transfer resistance is reduced. After going through the spiral baffle structure, the length of bubble is obviously decreased owing to the enhanced mass transfer. Nevertheless, the broken slug flow pattern, as reported by Yin et al. (2019b), has not been observed under our tested conditions.

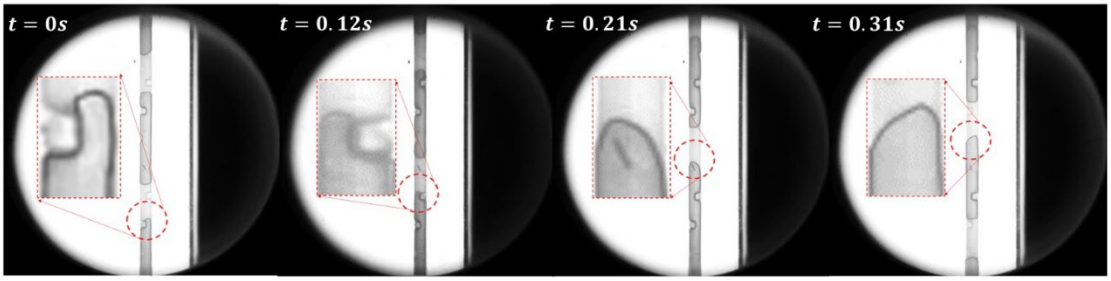

Figure 6 Typical bubble deformation in spiral baffle embedded microchannel captured by high-speed camera (Concitions: $Q_G = 168\ ml/h; Q_L = 30\ ml/h;\ C_{MEA} = 1\%$).

Fig. 7 shows the two-phase flow pattern map with the U_G and U_L as coordinate for CO_2 chemical absorption in smooth and spiral baffle structure embedded microchannels. The effects of baffle structure and absorbent concentration on the transition of flow patterns can be clearly seen. Firstly, higher C_{MEA} accelerates the reaction rate between the CO_2 and the MEA solution. The bubble volume shrinks very quickly, the bubbly flow/bubbly-slug flow becoming dominant on the flow map. In contrast, at low C_{MEA} (Fig. 7c), slug-annular flow can still be present in smooth microchannel as discussed above. Secondly, the presence of baffle structure results in smaller $l_{B,ini}$ (cf. Fig. 4 and Fig. 5) as well as the bubble deformation. As a result, the transition lines for the spiral baffle embedded microchannel are shifted to right compared to those for smooth microchannel, indicating the later transition from bubbly flow to bubbly-slug flow and from bubbly-slug flow to slug flow.

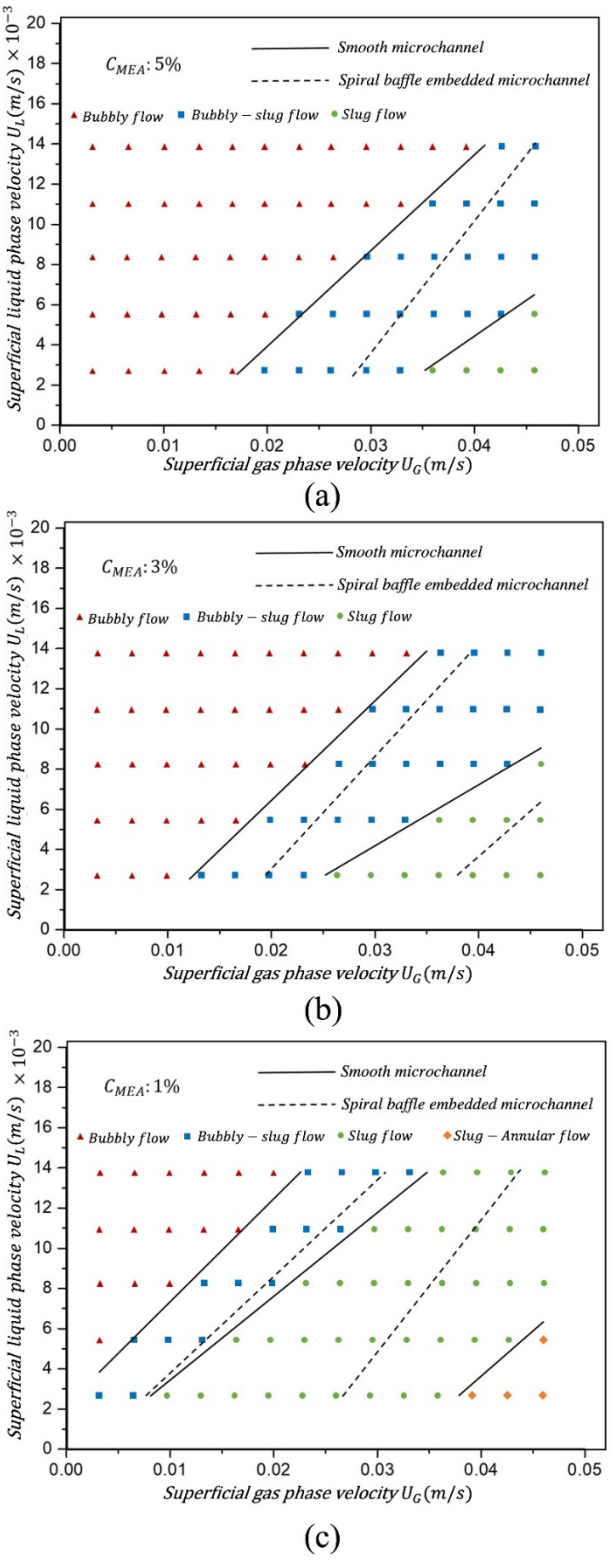

Figure 7 Two-phase flow map for CO_2 chemical absorption in smooth microchannel and in spiral baffle embedded microchannel. (a) C_{MEA}=5%; (b) C_{MEA}=3%; (c) C_{MEA}=1%.

3.2 CO_2 gas phase void fraction

CO_2 gas phase void fraction ($\mathrm{\Epsilon} = V_B/V_C$) is defined as the ratio of overall bubble volume (V_B) to the whole microchannel volume (V_C). It is an important parameter to predict the two-phase pressure drop and CO_2 mass transfer performance. In this study, the ε value has been estimated by image analysis method with some assumptions on the geometry of the slug bubble as explained in section 2.2. Due to the generation and the rapid contraction of CO_2 bubbles, the void fraction exhibits a repeated periodical fluctuation. As a result, the ε values reported here have been averaged within 20 s (including several periods from bubble generation to exhaust which is sufficiently long and representative). The results are shown in Fig. 8.

At a certain Q_L, ε value increases with the increasing Q_G, mainly due to the larger $l_{B,ini}$ as already shown in Fig. 4. Contrarily at a certain Q_G, ε value shows an upward trend with the decreasing Q_L. This is because of the lower liquid-side mass transfer coefficient at low Q_L. By comparing Figs. 8a-c, the positive effect of C_{MEA} on the reduction of ε can be clearly seen, mainly due to the stronger chemical reaction. Moreover, under the same testing condition, the ε value of spiral baffle embedded microchannel is always smaller than that of smooth microchannel, implying the higher mass transfer rate and the better absorption performance.

Further investigating the void fraction is meaningful for comprehensively understanding the two-phase hydrodynamic in microchannel (Yin et al. 2022b). Many prediction models have then been proposed at early stage, such as by Ali et al. (1993) (Eq. 18), Kawahara et al. (2002) (Eq. 19) and Saisorn & Wongwises (2009) (Eq. 20).

$$\varepsilon = 0.8\beta \tag{18}$$

$$\varepsilon = \frac{0.03\beta^{0.5}}{1 - 0.97\beta^{0.5}} \tag{19}$$

$$\varepsilon = \frac{0.036\beta^{0.5}}{1 - 0.945\beta^{0.5}} \tag{20}$$

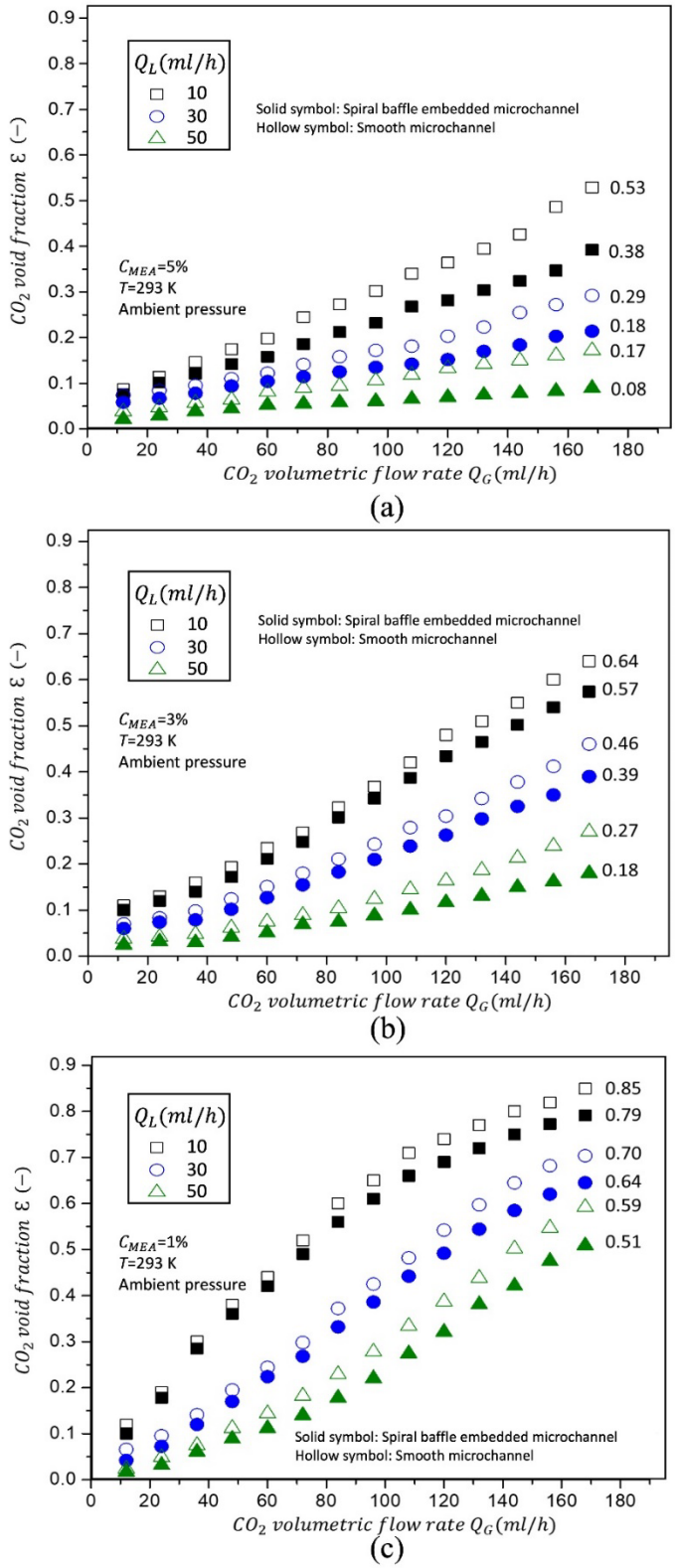

Figure 8 CO_2 gas phase void fraction (ε) in smooth and spiral baffle embedded microchannels. (a) $C_{MEA} = 5\%$; (b) $C_{MEA} = 3\%$; (c) $C_{MEA} = 1\%$.

Where $\beta = Q_G/(Q_G + Q_L)$. However, these models are only based on the gas and liquid flow rate ratio, thereby suited for two-phase flow systems without the chemical reaction (or when its effect could be ignored). Yin et al. (2018) proposed a modified model by adding the dimensionless Hatta number (Ha):

$$\varepsilon = \frac{0.8\beta}{1 + 5.3 \times 10^{-3} Ha} \tag{21}$$

$$Ha = \sqrt{D k_{ov} / {k_{L,P}}^2} \tag{22}$$

Where D (m^2/s) is the two-phase diffusion coefficient, k_{ov} $(1/s)$ is the overall chemical reaction rate, $k_{L,P}$ (m/s) is the liquid side physical mass transfer rate estimated by renewable mass transfer model.

Fig. 8 compares the experimental data of gas void fraction obtained in this study with the above-mentioned prediction models. A clear deviation can be seen. In fact, Ali's model is suitable for mini-scale flat plates channel reactor with stable two-phase split flow. The bubble volume decrease rate is small because of the limited mass transfer rate; thus the linear prediction correlation is proposed for this situation. Kawahara's model and Saisorn's model are proposed under the large gas and liquid superficial velocities ($U_G: 0.1 - 60\ m/s$, $U_L: 0.01 - 4\ m/s$) which lead to totally different flow patterns. For example, nearly single-phase flow was observed at high liquid flow rate for all gas flow rate, and for $\beta < 0.5$, the ε value remained smaller than 0.1. Thus, they cannot be used to predict the stable split flow (such as slug flow and bubbly flow) under small gas and liquid Re numbers tested in the present study. For correlation proposed by Yin et al. (2018), though the chemical reaction greatly promotes the two-phase mass transfer performance, the main channel length of their study is rather short (40 mm), resulting in the overestimation of ε. In this experiment with a longer microchannel accompanied with quick chemical reaction, the bubble volume change is realized within a shorter distance. For this reason, the current experimental ε data are generally smaller than the prediction values using Yin's model and shows a non-linear trend.

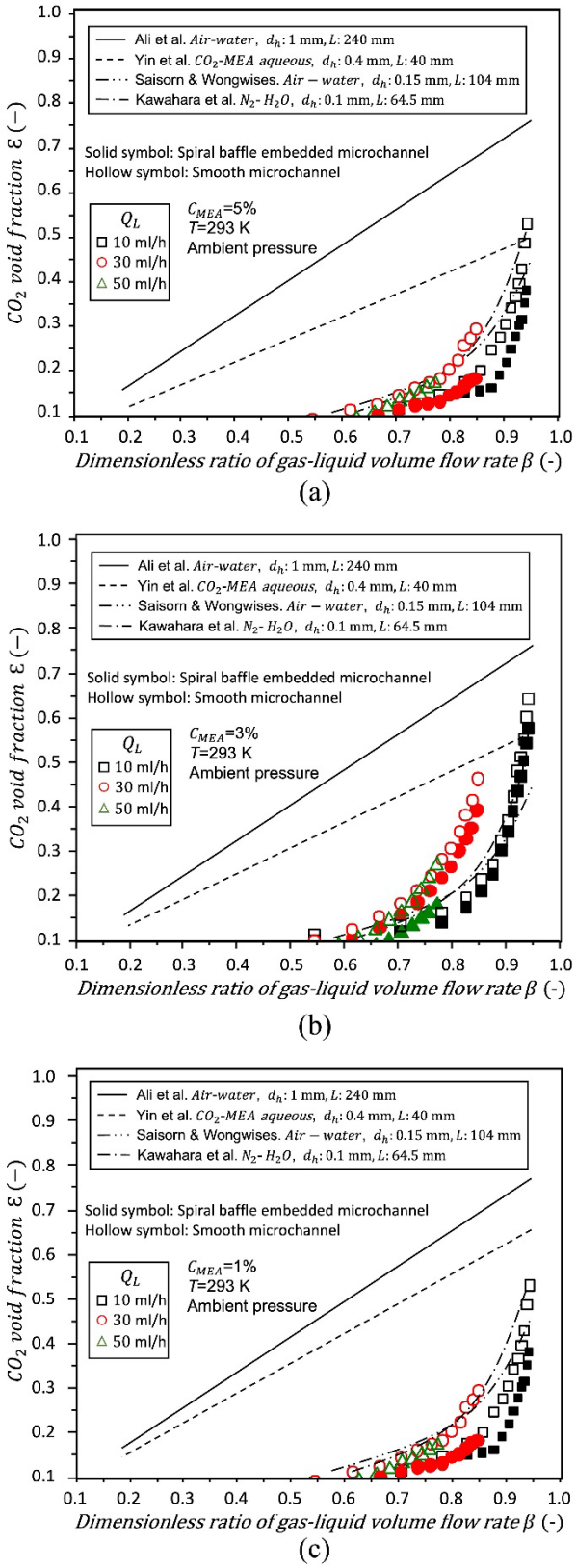

Figure 9 Comparison of CO_2 void fraction between the experimental data and calculated values by prediction models. (a) $C_{MEA} = 5\%$; (b) $C_{MEA} = 3\%$; (c) $C_{MEA} = 1\%$

Given the need of a new model for more accurate prediction of ε for CO_2 chemical absorption in microchannel at small gas and liquid Re numbers, the dimensionless Damköhler number (Da) is proposed to be included in the correlation to consider the effect of chemical reaction. The Da number is defined as the ratio of chemical reaction rate (k_{ov}) to the diffusion rate (D), expressed as follows (Ma et al., 2020):

$$Da = k_{ov} \cdot {d_h}^2 / D \tag{23}$$

For smooth microchannel, the new correlation could be written as follows:

$$\varepsilon_{smooth} = \frac{a\beta^b}{1 + c \cdot Da} \tag{24}$$

And based on the experimental data obtained in this study, the fitting factor a is 1.42, b is 3.22 and c is 1.93×10^{-6}.

For structured microchannel, the structure intensify factor (Ψ), Re_G and Re_L should also be considered to indicate the effects of flow disturbance structure on the CO_2 void fraction, written as:

$$\varepsilon_{structured} = (d{Re_G}^e {Re_L}^f)^{\Psi - 1} \varepsilon_{smooth} \tag{25}$$

Where the fitting constant is 0.006 for d, 2.856 for e and 0.17 for f, respectively, based on the results of this study. Ψ value for the spiral baffle structure is decided by the micro baffle dimension, the number and the distribution mode. It is estimated to be equal to 1.1 in this research while $\Psi = 1$ for the straight smooth microchannel case. Fig. 10 shows that the prediction values of ε using the new model are in good agreement with the experimental data, the maximum absolute error being smaller than ±25%.

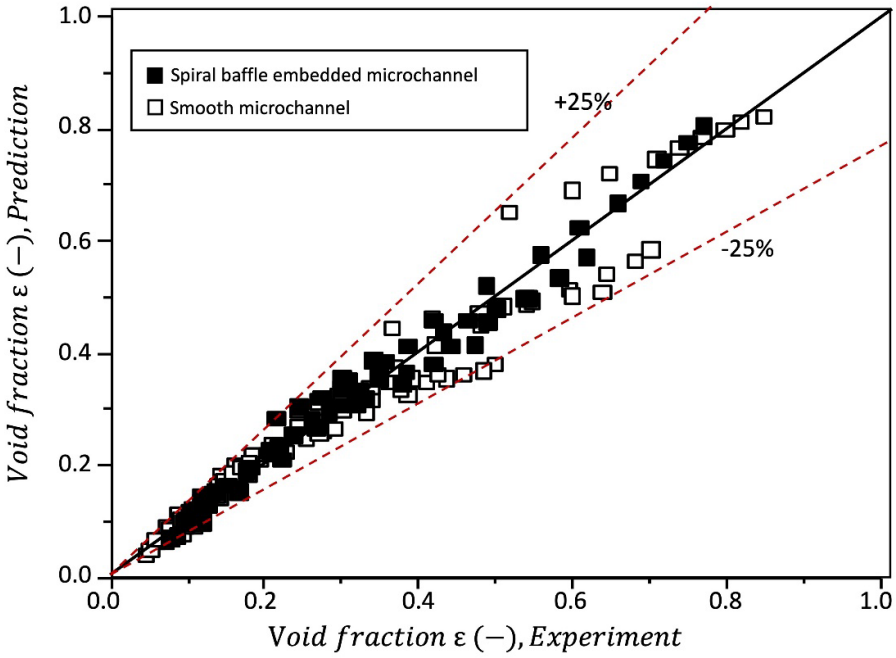

Figure 10 Predicted values of CO_2 void fraction compared with experimental data.

3.3 Pressure drop

Figure 11 shows the measured two-phase pressure drop (ΔP) for CO_2 chemical absorption by MEA solution in microchannel. From Fig. 11a, it can be seen that ΔP increases with the increasing Re_G and Re_L. The presence of the flow disturbance structure (spiral baffle) would cause an additional increase of ΔP, and this increase is more significant at high Re_G. The highest ΔP recorded under the tested conditions is about 750 Pa and the pressure drop increase due to the embedded spiral baffle is no more than 50 Pa, which is less than 10% and may be considered as acceptable in various industrial applications.

Figure 11b shows the effect of MEA solution concentration on the ΔP, indicating that the ΔP decreases with the increasing C_{MEA} under the same Re_L and Re_G condition. Given the almost constant physical properties of MEA solution within the tested concentration range (cf. Table 2), this difference in ΔP is mainly due to the different CO_2 absorption rate at different C_{MEA}. In fact, the lower ε value at high C_{MEA} would reduce the pressure drop caused by the bubble moving.

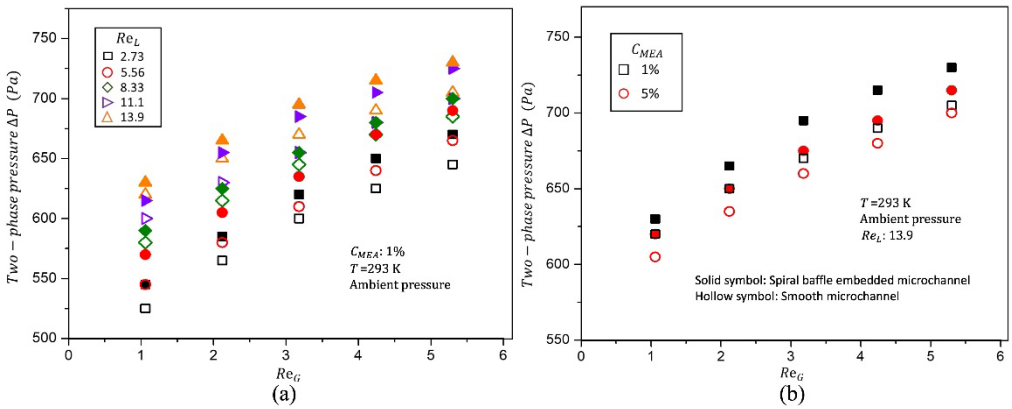

Figure 11 The measured two-phase pressure drop for CO_2 chemical absorption by MEA solution in smooth and spiral baffle embedded microchannels. (a) Influence of gas and liquid *Re* numbers; (b) Influence of MEA concentration.

3.4 Mass transfer performance

The effects of operating conditions (gas and liquid flow rates and MEA concentration) and spiral baffle structure on the mass transfer performance of CO_2 chemical absorption in microchannel are discussed here. Fig. 12 show the variation of $k_L a$ values under the tested conditions for smooth and spiral baffle embedded microchannels. The experimental results clearly show the dependence of $k_L a$ values on Re_G and Re_L, i.e., higher gas and liquid flow rates (or superficial velocities) enhance the mass transfer. Firstly, increasing the Re_G augments the mass of CO_2 on one hand, and promotes the transition from bubbly flow to slug flow on the other hand, which greatly increases the two-phase mass transfer surface area. Both effects would augment the $k_L a$. Moreover, increasing gas flow rate will shorten the liquid slug, which directly leads to an increase in shear force between liquid and solid, thereby promoting the liquid flow mixing at the meniscus position. Secondly, according to the surface renewal theory, the increased liquid superficial velocity could directly enhance the renewal rate of the absorbent around the CO_2 bubbles, thereby reducing the liquid side mass transfer resistance.

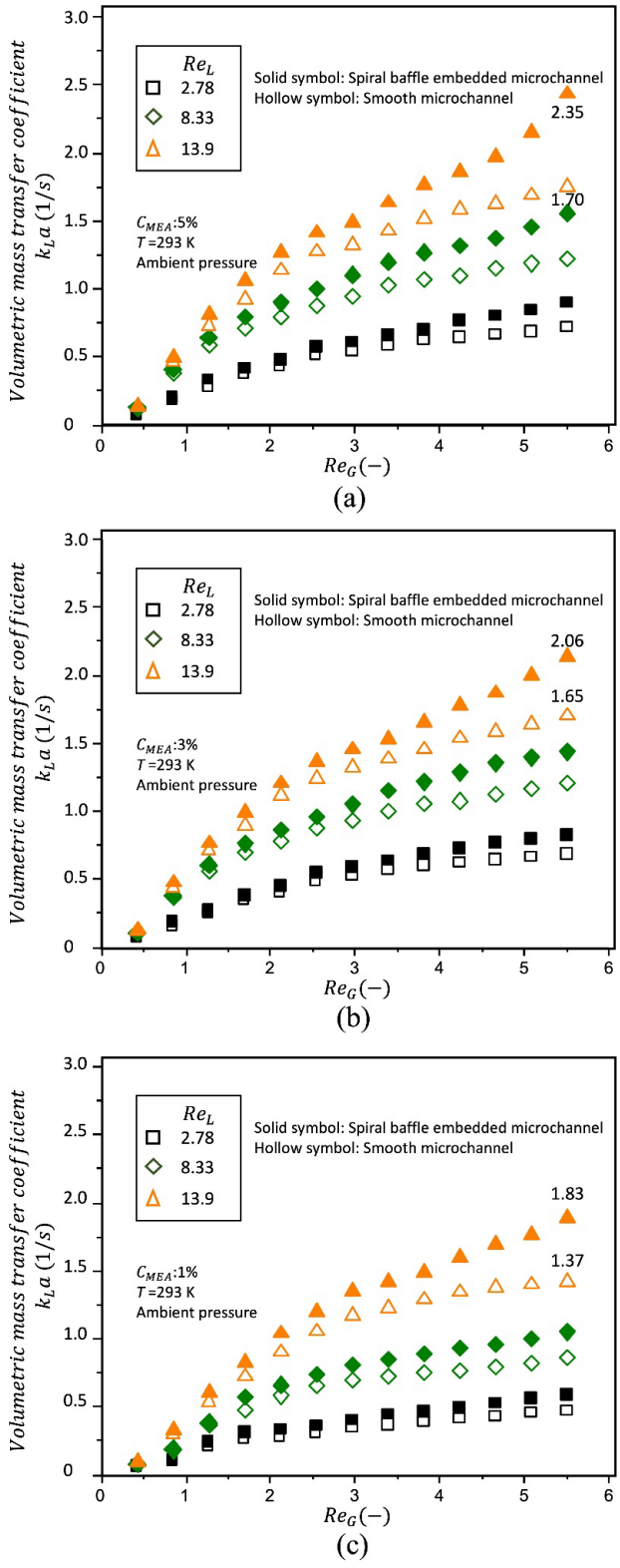

Figure 12 Effects of Re_G, Re_L, absorbent concentration and structure factor on liquid side volumetric mass transfer rate $k_L a$. (a) $C_{MEA} = 5\%$; (b) $C_{MEA} = 3\%$; (c) $C_{MEA} = 1\%$

In addition, the increasing C_{MEA} could directly increase the chemical reaction rate and decreasing the CO_2 molar concentration in the liquid phase correspondingly. The mass transfer process driven by the concentration difference is significantly enhanced and $k_L a$ obviously increased, especially at high Re_G. For smaller Re_G, the effect of C_{MEA} on the increase of $k_L a$ is less significant because of the decreased gas–liquid interfacial area for mass transfer.

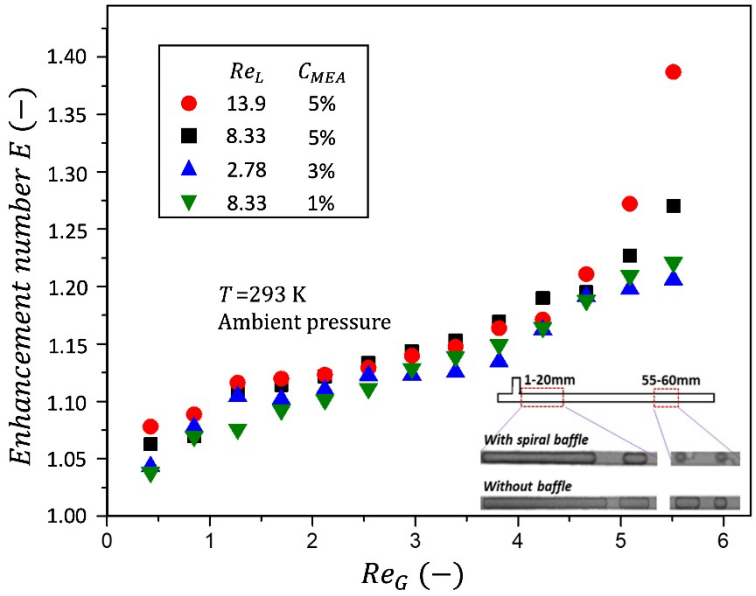

Figure 13 Enhancement number *E* achieved by spiral baffle structure.

Finally, the effect of spiral baffle structure on the enhancement of mass transfer is rather significant , indicated by the high values of E shown in Fig. 13. In smooth microchannel, the mass transfer is dominated by diffusion and the main convective mass transfer is happening at liquid phase meniscus position. The existence of spiral baffle structure could disturb the gas-liquid mass transfer interface and promote its renewal, thereby strengthening the CO_2 gas dissolve process. Besides, the spiral baffle structure could induce more spatially asymmetric vortices in liquid phase and this enhanced liquid mixing is more intensive at higher Re_L number, hence improving the chemical reaction rate and convective mass transfer. Both these two factors enhance the two-phase mass transfer performance. However, the enhancement achieved by the

spiral baffle structure varies with gas and liquid Re numbers. At low Re_L and Re_G numbers, the enhancement is relatively small because of the relatively weak disturbance when CO_2 bubbles pass through the spiral baffle structure. With the continuous increase of Re_L and Re_G numbers, k_La and E values are significantly augmented and the maximum value of k_La=2.35 s^{-1} and E=1.387 can be achieved. Such k_La values are 2-3 orders of magnitude higher than that of traditional devices (e.g., trickle bed reactor or packed column) at such small gas and liquid Re numbers ($Re_G < 5, Re_L < 15$) (Table 4), highlighting the interests of microchannel-based CO_2 chemical absorption devices. Besides, the novel spiral baffle structure also shows its effectiveness on the enhancement of mass transfer, especially for operations at small gas and liquid Re numbers.

Table 4 Comparison of k_La and E for different CO_2 chemical absorption devices within the given gas and liquid Re number range ($Re_G < 5, Re_L < 15$).

Type	k_La (s^{-1})	E	Ref
Trickle bed reactor	0.001-0.01		Larachi et al. (1998)
Packed column	0.001-0.05	-	Zeng et al. (2011)
Heart shape structured microreactor	0.53	1.12	Chen et al. (2021)
Rectangular baffles structured microreactor	2.1	1.27	Yin et al. (2020)
Spiral baffle embedded microchannel (This work)	Up to 2.35	Up to 1.387	

Plenty of semi-empirical correlations have been proposed for the prediction of mass transfer performance in mini/micro channel-based CO_2 absorber. For example, the correlation of Yue et al. (2007b) for slug flow (Eq. 26) and for slug-annular flow (Eq. 27), and the correlation of Ji et al. (2010) for slug flow (Eq. 28) are shown as below

$$Sh_L \cdot a \cdot d_h = 0.084 {Re_G}^{0.213} \cdot {Re_L}^{0.937} \cdot {Sc_L}^{0.5} \quad (26)$$

$$Sh_L \cdot a \cdot d_h = 0.058 {Re_G}^{0.344} \cdot {Re_L}^{0.912} \cdot {Sc_L}^{0.5} \quad (27)$$

$$Sh_L \cdot a \cdot d_h = 0.22 {Re_G}^{0.78} \cdot {Re_L}^{0.0535} \cdot Sc_L \cdot {Ca_L}^{0.7568} \quad (28)$$

Where Sh is the Sherwood number ($Sh_L = k_L \cdot d_h / D$) and Sc is the Schmidt number ($Sc_L = \mu_L / (D \cdot \rho_L)$

Nevertheless, these correlations were developped for CO_2-H_2O system, thus can better predict the CO_2 physical absorption. For CO_2 chemical absorption (MEA solution) in microchannel, empirical correlations have also been proposed by Li et al. (2014) (Eqs. 29, 30) for the operation condition ($26.73 < Re_G < 467.79$ and $5.35 < Re_L < 37.42$) and by Yin et al. (2019a) (Eq. 31) for the operation condition ($1.29 < Re_G < 9.44$ and $11.68 < Re_L < 31.68$):

$$Sh_L \cdot a \cdot d_h = 5.0107 Re_G^{2.9423} \cdot Re_L^{-1.5583} \cdot Sc_L^{0.5} \cdot Ca_L^{0.0743} \quad \frac{Re_G}{Re_L} < 1.7319 \tag{29}$$

$$Sh_L \cdot a \cdot d_h = 19.389 Re_G^{0.3872} \cdot Re_L^{0.8865} \cdot Sc_L^{0.5} \cdot Ca_L^{0.4176} \quad \frac{Re_G}{Re_L} \geq 1.7319 \tag{30}$$

$$Sh_L \cdot a \cdot d_h = 0.81 \cdot Re_G^{0.78} \cdot Re_L^{0.41} \cdot Da^{0.35} \tag{31}$$

Specifically for intensified microchannels, the enhancement number E has been proposed to be added into the correlation Chu et al. (2019):

$$Sh_L \cdot a \cdot d_h = 1.3425 \cdot Re_G^{1.0968} \cdot Re_L^{-0.4705} \cdot Sc_L^{0.5} \cdot Ca_L^{-0.0302} \cdot E^{0.7198} \tag{32}$$

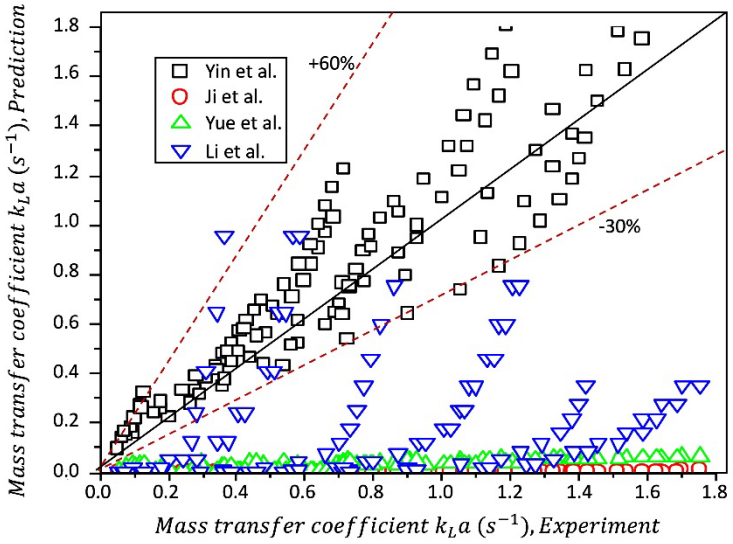

Figure 14 Comparison of k_La value between the experimental data in smooth microchannel and prediction values by related correlations.

Fig. 14 shows a comparison of experimental data for smooth microchannel obtained in this study with the prediction results using the above-mentioned correlations. Large deviations can be seen for correlations based only on physical parameters. For Yin et al. (2019a)'s correlation

that includes the Da number, the prediction error could be significantly reduced, but could still reach -30% to 60%. This is because Yin et al. (2019a)'s correlation has been proposed for Re_L number range $(11.68 - 31.68)$ and Re_G number range (1.29-9.44), two times larger than that of this study. Besides, the above mass transfer prediction model did not consider the effect of intensification micro-structure on the mass transfer performance. As a result, proper mass transfer prediction correlations that consider chemical reaction and intensification structure for small Re_G and Re_L numbers range are still lacking.

Therefore, new correlations are proposed based on the experimental data obtained in this study. In particular, the Da number and the E number have been included to consider the effect of chemical reaction and intensification structure on the enhancement of mass transfer, shown in Eq. 33 and Eq. 34.

$$Sh_L \cdot a \cdot d_h = 6.45 \cdot {Re_G}^{0.6234} \cdot {Re_L}^{0.628} \cdot Da^{0.16} \cdot E \tag{33}$$

$$E = ({Re_G}^{0.512} {Re_L}^{-0.026} Da^{0.07})^{\Psi-1} \tag{34}$$

From these correlations, it can be seen that for the smooth channel, both Re_G and Re_L have almost the equal effect on the improvement of mass transfer. The positive impact of solvent concentration (Da) can also be well recognized. For the structured microchannel, the enhancement is much more sensitive to Re_G than others under our tested conditions.

Fig. 15 shows that the experimental data and the prediction results of the new model are in good agreement: the relative error is below ±15% for E number and below ±20% for $k_L a$, respectively.

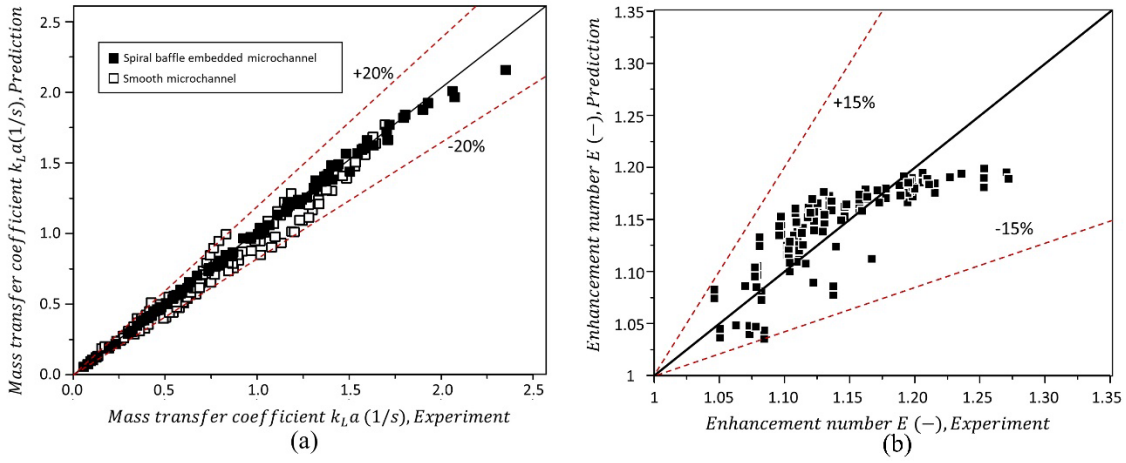

Figure 15 Comparison of experimental data with new prediction model. (a) Liquid side volumetric mass transfer rate k_La. (b) Mass transfer enhancement number E.

3.5 Effective energy efficiency

Undoubtedly, adding micro intensification structures will increase the two-phase pressure drop, but it also enhances the two-phase mass transfer performance. In order to further estimate the mass transfer enhancement efficacy, the parameter effective energy efficiency (η) is introduced here for analysis (Li et al., 2019). η is defined as the ratio of mass transfer enhancement number (E) to the energy consumption ratio, expressed in Eq.35. Ec is micro CO_2 absorber energy consumption and calculated as Eq.36 (Chen et al., 2021):

$$\eta = \frac{E}{Ec_{structured}/Ec_{Smooth}} \tag{35}$$

$$Ec = \frac{\Delta P \cdot (Q_G + Q_L)}{V_c \rho_L} \tag{36}$$

Where ΔP is two-phase pressure drop, ρ_L is the liquid phase density and estimated here as constant. Fig.16a shows the effect of gas or liquid flow rate and absorbent concentration on energy consumption for two tested microchannels. It could be found that the Ec values increase with the increasing gas-liquid flow rates and the largest Ec is no more than 0.5 $W\ /\ kg$ within our tested conditions. Compared with smooth microchannel, the Ec slightly increased. It is

worth noting that the impact of absorbent concentration on the energy consumption is far less significant than that of gas or liquid flow rate.

The influence of gas or liquid flow rate and absorbent concentration on the effective energy efficiency η is shown in Fig.17. It can be seen that the value of η clearly increases with the gas flow rate, owing to the quickly increased E.

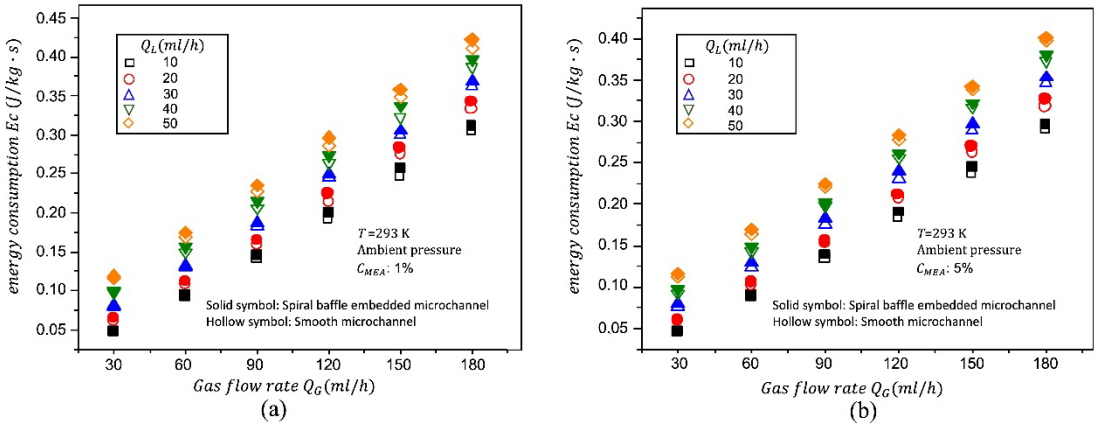

Figure 16 Effect of gas or liquid flow rate and absorbent concentration on the energy consumption Ec. (a) $C_{MEA} = 1\%$; (b) $C_{MEA} = 5\%$.

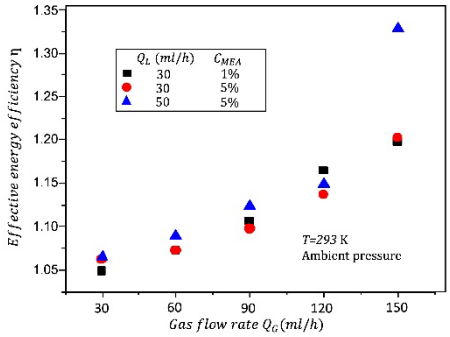

Figure 17 Effect of gas or liquid flow rate and absorbent concentration on the effective energy efficiency η.

4. Conclusion

In this study, CO_2-MEA mass transfer performance in microchannel-based absorber has been experimentally evaluated. In particular, a novel spiral baffle structure has been embedded in the

straight microchannel to enhance the gas-liquid mass transfer. Results show that the existence of spiral baffle structure could induce the CO_2 bubble deformation, thereby disturbing the gas-liquid mass transfer interface and promoting its renewal. Besides, more spatially asymmetric vortices in liquid phase could be formed to enhance the liquid mixing, hence improving the chemical reaction rate and convective mass transfer. With the increase of gas and liquid flow rates, the induced vortex intensity could also be augmented. Compared with the straight smooth microchannel, better CO_2 absorption performance can be achieved owing to the spiral baffle structure, with $k_L a$ value up to 2.35 s^{-1} and enhancement number E up to 1.387 under the tested conditions. This mass transfer enhancement achieved in small gas and liquid Re number range ($Re_G < 5.5$ and Re_L <14) is particularly interesting because of the small pressure drop increase (<10%) compared to the smooth microchannel. The results show that largest energy consumption (Ec) is no more than 0.5 W / kg and effective energy efficiency (η) gradually increased within the gas-liquid flow operating range. Based on the obtained experimental data, new models and correlations have been proposed for predicting the gas void fraction (ε), the enhancement number (E) and the liquid-side mass transfer coefficient ($k_L a$) at small gas and liquid Re numbers. The effects of chemical reaction (solvent concentration) and intensification structure have been taken into account by including the Da number and Ψ factor into the models/correlations. Good agreement has been achieved between the experimental data and prediction results, with the maximum absolute error smaller than 25% under the tested conditions.

Acknowledgement

This work is supported by the China Scholarship Council with the scholarship for Mr. Hao CHENG (No. 20200673006) and by the French Ministry of Europe and Foreign Affairs (Ministère de l'Europe et des Affaires Étrangères) through the PHC Xu Guangqi program (No.45614RM, 2020). One of the authors, Y. Fan, would like to thank Dr. Bin CAO at Xi'an Shiyou University (China) for the fruitful discussions and helpful suggestions.

References

Ali, M.I., Sadatomi, M., Kawaji, M., 1993. Adiabatic two-phase flow in narrow channels between two flat plates. Can. J. Chem. Eng. 71, 657–666.

Chen, S., Zhang, T., Lv, L., Chen, Y., Yang, Y., Tang, S., 2019. Intensification of the liquid side mass transfer in double-side falling film microchannels by micro-mixing structures. Chem. Eng. Sci. 193, 264–275.

Chen, Y., Zhu, C., Fu, T., Ma, Y., 2021. Mass transfer enhancement of CO2 absorption into [Bmim][BF4] aqueous solution in microchannels by heart-shaped grooves. Chem. Eng. Process. Intensif. 167, 108536.

Cheng, H., Fan, Y., Tarlet, D., Luo, L., Fan, Z., 2023. Microfluidic-based chemical absorption technology for CO2 capture: Mass transfer dynamics, operating factors and performance intensification. Renew. Sustain. Energy Rev. 181, 113357. https://doi.org/10.1016/j.rser.2023.113357

Chu, C., Zhang, F., Zhu, C., Fu, T., Ma, Y., 2019. Mass transfer characteristics of CO2 absorption into 1-butyl-3-methylimidazolium tetrafluoroborate aqueous solution in microchannel. Int. J. Heat Mass Transf. 128, 1064–1071.

Dong, Z., Yao, C., Zhang, X., Xu, J., Chen, G., Zhao, Y., Yuan, Q., 2015. A high-power ultrasonic microreactor and its application in gas–liquid mass transfer intensification. Lab Chip 15, 1145–1152.

Florides, G.A., Christodoulides, P., 2009. Global warming and carbon dioxide through sciences. Environ. Int. 35, 390–401.

Ji, X.Y., Ma, Y.G., Fu, T.T., Zhu, C.H., Wang, D.J., 2010. Experimental investigation of the liquid volumetric mass transfer coefficient for upward gas-liquid two-phase flow in rectangular microchannels. Brazilian J. Chem. Eng. 27, 573–582.

Kashid, M.N., Renken, A., Kiwi-Minsker, L., 2011. Gas–liquid and liquid–liquid mass transfer in microstructured reactors. Chem. Eng. Sci. 66, 3876–3897.

Kawahara, A., Chung, P.-Y., Kawaji, M., 2002. Investigation of two-phase flow pattern, void fraction and pressure drop in a microchannel. Int. J. Multiph. flow 28, 1411–1435.

Koytsoumpa, E.I., Bergins, C., Kakaras, E., 2018. The CO2 economy: Review of CO2 capture and reuse technologies. J. Supercrit. Fluids 132, 3–16.

Lamb, K.J., 2017. Investigating Alternative Green Methods for Carbon Dioxide Utilisation and Carbon Capture and Storage.

Larachi, F., Cassanello, M., Laurent, A., 1998. Gas− liquid interfacial mass transfer in trickle-bed reactors at elevated pressures. Ind. Eng. Chem. Res. 37, 718–733.

Li, C., Zhu, C., Ma, Y., Liu, D., Gao, X., 2014. Experimental study on volumetric mass transfer coefficient of CO2 absorption into MEA aqueous solution in a rectangular microchannel reactor. Int. J. Heat Mass Transf. 78, 1055–1059.

Li, G., Pu, X., Shang, M., Zha, L., Su, Y., 2019. Intensification of liquid–liquid two-phase mass transfer in a capillary microreactor system. AIChE J. 65, 334–346.

Lin, G., Jiang, S., Zhu, C., Fu, T., Ma, Y., 2019. Mass-transfer characteristics of CO2 absorption into aqueous solutions of N-methyldiethanolamine+ diethanolamine in a T-junction microchannel. ACS Sustain. Chem. Eng. 7, 4368–4375.

Lv, B., Guo, B., Zhou, Z., Jing, G., 2015. Mechanisms of CO2 capture into monoethanolamine solution with different CO2 loading during the absorption/desorption processes. Environ. Sci. Technol. 49, 10728–10735.

Ma, D., Zhu, C., Fu, T., Yuan, X., Ma, Y., 2020. An effective hybrid solvent of MEA/DEEA for CO2 absorption and its mass transfer performance in microreactor. Sep. Purif. Technol. 242, 116795.

Mc Carogher, K., Dong, Z., Stephens, D.S., Leblebici, M.E., Mettin, R., Kuhn, S., 2021. Acoustic resonance and atomization for gas-liquid systems in microreactors. Ultrason. Sonochem. 75, 105611.

Moffat, R.J., 1988. Describing the uncertainties in experimental results. Exp. Therm. Fluid Sci. 1, 3–17. https://doi.org/10.1016/0894-1777(88)90043-X

Murai, S., Fujioka, Y., 2008. Challenges to the carbon dioxide capture and storage (CCS) technology. IEEJ Trans. Electr. Electron. Eng. 3, 37–42.

Nie, X., Zhu, C., Fu, T., Ma, Y., 2022. Mass transfer intensification and mechanism analysis of gas–liquid two-phase flow in the microchannel embedding triangular obstacles. Chinese J. Chem. Eng. 51, 100–108.

Niu, H., Pan, L., Su, H., Wang, S., 2009. Flow pattern, pressure drop, and mass transfer in a gas− liquid concurrent two-phase flow microchannel reactor. Ind. Eng. Chem. Res. 48, 1621–1628.

Pang, Z., Jiang, S., Zhu, C., Ma, Y., Fu, T., 2021. Mass transfer of chemical absorption of CO2 in a serpentine minichannel. Chem. Eng. J. 414, 128791.

Pasha, M., Liu, S., Zhang, J., Qiu, M., Su, Y., 2022. Recent Advancements on Hydrodynamics and Mass Transfer Characteristics for CO2 Absorption in Microreactors. Ind. Eng. Chem. Res.

Saisorn, S., Wongwises, S., 2009. An experimental investigation of two-phase air–water flow through a horizontal circular micro-channel. Exp. Therm. Fluid Sci. 33, 306–315.

Schreyer, F., Luderer, G., Rodrigues, R., Pietzcker, R.C., Baumstark, L., Sugiyama, M., Brecha, R.J., Ueckerdt, F., 2020. Common but differentiated leadership: strategies and challenges for carbon neutrality by 2050 across industrialized economies. Environ. Res. Lett. 15, 114016.

Shakun, J.D., Clark, P.U., He, F., Marcott, S.A., Mix, A.C., Liu, Z., Otto-Bliesner, B., Schmittner, A., Bard, E., 2012. Global warming preceded by increasing carbon dioxide concentrations during the last deglaciation. Nature 484, 49–54.

Stewart, C., Hessami, M.A., 2005. A study of methods of carbon dioxide capture and sequestration - The sustainability of a photosynthetic bioreactor approach. Energy Convers. Manag. 46, 403–420. https://doi.org/10.1016/j.enconman.2004.03.009

Tan, J., Lu, Y.C., Xu, J.H., Luo, G.S., 2012. Mass transfer characteristic in the formation stage of gas–liquid segmented flow in microchannel. Chem. Eng. J. 185, 314–320.

TeGrotenhuis, W.E., Cameron, R.J., Viswanathan, V. V, Wegeng, R.S., 2000. Solvent extraction and gas absorption using microchannel contactors, in: Microreaction Technology: Industrial Prospects. Springer, pp. 541–549.

Versteeg, G.F., Van Swaaij, W.P.M., 1988. Solubility and diffusivity of acid gases (carbon dioxide, nitrous oxide) in aqueous alkanolamine solutions. J. Chem. Eng. Data 33, 29–34.

Whitman, W.G., 1923. The two-film theory of gas absorption. Chem. Met. Eng. 29, 146–148.

Yin, Y., Chen, W., Wu, C., Zhang, X., Fu, T., Zhu, C., Ma, Y., 2022a. Bubble dynamics and mass transfer enhancement in split–and–recombine (SAR) microreactor with rapid chemical reaction. Sep. Purif. Technol.

120573.

Yin, Y., Chen, W., Zhu, X., Zhu, C., Fu, T., Zhang, X., Ma, Y., 2022b. Effect of solvent on CO2 absorption performance in the microchannel. J. Mol. Liq. 357, 119133.

Yin, Y., Fu, T., Zhu, C., Guo, R., Ma, Y., Li, H., 2019a. Dynamics and mass transfer characteristics of CO2 absorption into MEA/[Bmim][BF4] aqueous solutions in a microchannel. Sep. Purif. Technol. 210, 541–552.

Yin, Y., Guo, R., Zhu, C., Fu, T., Ma, Y., 2020. Enhancement of gas-liquid mass transfer in microchannels by rectangular baffles. Sep. Purif. Technol. 236, 116306.

Yin, Y., Zhu, C., Fu, T., Ma, Y., Wang, K., Luo, G., 2019b. Enhancement effect and mechanism of gas-liquid mass transfer by baffles embedded in the microchannel. Chem. Eng. Sci. 201, 264–273.

Yin, Y., Zhu, C., Guo, R., Fu, T., Ma, Y., 2018. Gas-liquid two-phase flow in a square microchannel with chemical mass transfer: Flow pattern, void fraction and frictional pressure drop. Int. J. Heat Mass Transf. 127, 484–496. https://doi.org/10.1016/j.ijheatmasstransfer.2018.07.113

Youn, Y.J., Muramatsu, K., Han, Y., Shikazono, N., 2015. The effect of initial flow velocity on the liquid film thickness in micro tube accelerated slug flow. Int. J. Multiph. Flow 73, 108–117.

Yue, J., Chen, G., Yuan, Q., Luo, L., Gonthier, Y., 2007. Hydrodynamics and mass transfer characteristics in gas-liquid flow through a rectangular microchannel. Chem. Eng. Sci. 62, 2096–2108. https://doi.org/10.1016/j.ces.2006.12.057

Zanfir, M., Gavriilidis, A., Wille, C., Hessel, V., 2005. Carbon dioxide absorption in a falling film microstructured reactor: experiments and modeling. Ind. Eng. Chem. Res. 44, 1742–1751.

Zeng, Q., Guo, Y., Niu, Z., Lin, W., 2011. Mass transfer coefficients for CO2 absorption into aqueous ammonia solution using a packed column. Ind. Eng. Chem. Res. 50, 10168–10175.

Zhang, S., Zhu, C., Feng, H., Fu, T., Ma, Y., 2021. Intensification of gas-liquid two-phase flow and mass transfer in microchannels by sudden expansions. Chem. Eng. Sci. 229, 116040.

Zhu, C., Lu, Y., Fu, T., Ma, Y., Li, H.Z., 2017. Experimental investigation on gas-liquid mass transfer with fast chemical reaction in microchannel. Int. J. Heat Mass Transf. 114, 83–89.